Study on Electrostatic Ion Cyclotron Waves in Multi-Ions around the Cusp Region

Vibhooti khaira[#1] and G. Ahirwar*[2]
School of studies in physics,
Vikram university, Ujjain (M.P.) 456010, India

Abstract

Electrostatic ion-cyclotron waves are inspected with multi-ion plasma (H^+, He^+ and O^+) using particle aspect analysis. The plasma is deliberated to contain of resonant and non-resonant particles. The resonant particles contribute in energy conversationalthough the non-resonant particles provision the oscillatory motion of the wave. The wave is supposed to propagate explicitly to the static magnetic field. Dispersion relation, growth rate, parallel and perpendicular resonant energy have been scrutinized for electrostatic ion-cyclotron waves with multi-component plasma. The influence of kappa distribution function with fluctuating plasma density is to enrich the growth rate of EIC waves with multi- component plasma (H^+, He^+ and O^+). The kappa distribution acts as source of free energy. The fallouts are inferred for the space plasma parameters applicable to the cusp region nearby the earth's magnetosphere. The schoolwork may clarify the EIC waves detected in cusp region and play a most important role of particle density variation in particular region.

Keyword: *Electrostatic ion cyclotron wave, cusp region, multi-ions plasma, kappa distribution, temperature anisotropy, growth rate, dispersion relation.*

1. INTRODUCTION

The cusp region is usually defined as the regions of the magnetosphere in which magnetosheath plasma has direct entry in the ionosphere (Russell, 2000b). The cusp dynamics and the transient phenomena that occur in the high-latitude dayside ionosphere under southward IMF have been widely reported. The northward IMF case, however, was less talked about in the literature until very recently. In particular, multiinstrument studies involving ground-based facilities are still *Correspondence to:* F. Pitout (fp@irfu.se) rare (e.g. Maynard et al., 2000; Pryse et al., 2000; Sandholt et al., 1999a).

The FAST satellite crossing the polar cusp at 2000 km altitude has perceived the electrostatic emissions at a wide range of frequencies [1]. Remarks by Viking and other satellites have also revealedautographs of EIC waves with mountaintops in the power spectrum near the proton gyro frequency, in the cusp region [2]. Current data investigation of Cluster satellite has also revealedautographs of local ion-cyclotron waves in the cusp region [3]. Plasma particles in the cusp region, due to the curved and converging field lines, have precise high anisotropies in their transverse and parallel velocity components and thus, substantiallyproceed from the Maxwellian distribution and have the kappadistribution of particles [1, 4-6]. The authors have previously used the loss-cone distribution function to study the EICI in the auroral acceleration region [5, 6]. In the present paper, EIC wave with kappa distribution function is studied in the cusp region using the particle aspect analysis approach [4-7].

In this paper, we have seen the effect of kappa distribution function on electrostatic ion cyclotron wave in multi-ion plasma for cusp region by using particle aspect analysis. The detailed description and formulae for the dispersion relation and growth rate is determined in the subsequent section.

II. BASIC ASSUMPTION

The trajectories of particles are then evaluated within the framework of linear theory.

$$K_{\Pi} E, k = (k_{\perp}, 0, k_{\Pi}) \; , \; E = (E_x, 0, E_z)$$

With

$$E_x(r,t) = E_1 \cos(k_{\perp} x + k_{\Pi} z - \omega t),$$

$$E_z(r,t) = kE_1 \cos(k_{\perp} x + k_{\Pi} z - \omega t)$$

and

$$k = \left(\frac{k_{\Pi}}{k_{\perp}}\right) < 1$$

where

$$\phi = k_{\perp} x + k_{\Pi} z - \omega t$$

The amplitude E_1 is slowly varying function of t i.e

$$\frac{1}{E_1}\left(\frac{dE_1}{dt}\right) << \omega$$

Here, k_{II} and $k_{\perp}$ are the components of the wave vector along and across the magnetic field, respectively and ω represent the wave frequency.

A. Velocities of the particle

The trajectories of particles are evaluated within the framework of linear theory. The equation of motion of a particle is given by,

$$m\left(\frac{dv}{dt}\right) = q[E + \left(\frac{1}{c}\right)v \times B_0] \qquad (1)$$

If E is considered to be a small perturbation i.e. $E=E_0+E_1$, velocity v can be expressed in terms of unperturbed velocity V and perturbed velocity u.
Then the trajectories of the free gyration are obtained as;

$$X(t) = \frac{V_{\perp}}{\Omega_{\alpha}}[\sin(\theta - \Omega_{\alpha} t) - \sin\theta] + Y_{0,}$$

$$Y(t) = \frac{V_{\perp}}{\Omega_{\alpha}}[\cos(\theta - \Omega_{\alpha} t) - \cos\theta] + Y_{0,}$$

$$Z(t) = V_{\Pi} t + Z_{0,}$$

(2)

The perturbed velocity u is determined by;

$$\frac{du_{\perp}}{dt} + i\Omega_{\alpha} u_{\perp} = \frac{qk_{II}E_1}{k_{\perp}m}\sum_{-\infty}^{+\infty} J_1(\mu)\cos(A_{\lambda}t + \psi_{\lambda}^{0})$$

$$\frac{du_{\Pi}}{dt} = \frac{qE_1}{m}\sum_{-\infty}^{+\infty} J_1(\mu)\cos(A_{\lambda}t + \psi_{\lambda}^{0})$$

(3)

Where $u_{\perp} = u_x + iu_y$ represents the perturbed velocity in transverse direction and $u_{\parallel}$ represents the velocity in parallel direction. The resonance criteria are given by;

$$A_{\lambda}(V_{\Pi} = V_r) = k_{II}V_{II} - \omega + \lambda\Omega_{\alpha} = 0; \lambda = \pm1, \pm2, \pm3, \ldots\ldots \ldots\ldots$$

Here, V_r is the resonance velocity of the particles.
The oscillatory solution of u (t) is given by;

$$u_x(\vec{r}.t) = -\frac{qE_1}{m}\sum_{-\infty}^{+\infty} J_n(\mu)\times\left[\frac{A_{\lambda}}{A_{\lambda} - \Omega^2_{\alpha}}\sin\chi_{nl} - \frac{\delta}{2A_{n+1}}\sin(\chi_{nl} - A_{n+1}t)\right.$$

$$\left. - \frac{\delta}{2A_{n-1}}\sin(\chi_{nl} - A_{n-1}t)\right]$$

$$u_y(\vec{r}.t) = \frac{qE_1}{m}\sum_{-\infty}^{+\infty} J_n(\mu)\sum_{-\infty}^{+\infty} J_{\lambda}(\mu)\times\left[\frac{A_{\lambda}}{A^2_{\lambda} - \Omega^2_{\alpha}}\cos\chi_{nl}\right.$$

$$\left. - \frac{\delta}{2A_{n+1}}\cos(\chi_{nl} - A_{\lambda+1}t) - \frac{\delta}{2A_{\lambda-1}}\sin(\chi_{nl} - A_{\lambda-1}t)\right]$$

$$u_z(\vec{r}.t) = \frac{qk_{II}E_1}{k_{\perp}m}\sum_{-\infty}^{+\infty} J_n(\mu)\sum_{-\infty}^{+\infty} J_{\lambda}(\mu)\times\frac{1}{A_{\lambda}}[\sin\chi_{nl} -$$

(4)

$$\delta\sin(\chi_{nl} - A_{n+1}t)]$$

Here

$$\chi_{nl} = k.r - \omega t + (n - \lambda)(\Omega_{\alpha} t - \theta)$$

δ =0 for non-resonant particles and δ =1for resonant particles.

B. Distribution Function

To determine the dispersion relation and growth rate, we consider bi-Maxwellian plasma as,

$$f_0(y, V) = N_0 f_{\perp}(V_{\perp}) f_{\Pi}(V_{\Pi}) \qquad (5)$$

We consider a general loss-cone distribution function for $f_{\perp}(V_{\perp})$ as

$$f_{\perp}(V_{\perp}) = \left[\frac{V^{2J}_{\perp}}{\pi V^{2(J+1)}_{T\perp}}\right]\exp\left(-\frac{V^2_{\perp}}{V^2_{T\perp}}\right) \qquad (6)$$

And $f_{\parallel}(V_{\parallel})$ which is defined by the drifting Maxwellian as $f_{II}(V_{II}) = \left[\frac{V^{2J}_{II}}{\sqrt{\pi} V^{2(J+1)}_{II\perp}}\right]\exp\left(-\frac{V^2_{II}}{V^2_{III}}\right)$ (7)

Here using the value of $V^2_{T\perp} = (J+1)^{-1}\frac{2T_{\perp}}{m}$ and $V^2_{III} = \frac{2T_{II}}{m}$ for plasma and the bi-lorentzian, which reduces to the anisotropic bi-maxwellian distribution when the spectral index k tends to infinity is given by,

$$F = \frac{1}{\sqrt[3]{\pi}}\frac{\Gamma(\kappa + J + 1)}{\sqrt[3]{\kappa}\,\Gamma\kappa - 1/2 V^2_{T\perp} V^2_{III}}$$

$$[1 + \frac{V^2_{T\perp}}{KV^2_{T\perp}} + \frac{V^2_{III}}{KV^2_{III}}]^{-(\kappa+J+1)}$$

(8)

In equation (8) $V^2_{T\perp}$ and V^2_{III} are related to the mass m and the temperatures $T_{\perp}$ and T_{II} respectively parallel and perpendicular to the magnetic field by,

$$V^2_{T\perp} = (J+1)^{-1}[\frac{\kappa - 3/2}{\kappa}\frac{2KT_{\perp}}{m}] \qquad (9)$$

$$V^2_{III} = [\frac{\kappa - 3/2}{\kappa}\frac{2KT_{II}}{m}] \qquad (10)$$

The quasi-neutrality condition yields to the equation:

$$n_e = n_{H^+} + n_{He^+} + n_{O^+}$$

Thus we evaluate the density perturbation associated with the particle velocity as:

$$\frac{dn_1}{dt} = -F_{H^+}(V)(\nabla.u)_{H^+} + (-F_{He^+}(V)(\nabla.u)_{He^+}$$

$$+ (-F_{O^+}(V)(\nabla.u)_{O^+}$$

(11)

The integration w.r.to t from equation (8) we get the solution for perturbed density as

$$n_1(r,t) = -\frac{qE_1F(V_\alpha)}{m_\alpha k_\perp^2} k_{II}^2 \sum_{-\infty}^{+\infty} J_\lambda(\mu) J_n(\mu) \times$$

$$[\frac{k_\perp}{A_\lambda^2 - \Omega_\alpha^2} + \frac{k_{II}^2 K_\perp}{k_\perp^2 A_\lambda^2}] \sin \chi_{nl}$$

And

$$n_1(r,t) = \frac{qE_1F(V_{H^+})}{m_{H^+}k_\perp^2} k_{II}^2 K_\perp \sum_{\lambda,n=-\infty}^{+\infty} J_\lambda(\mu) J_n(\mu)$$

$$\frac{1}{A_{\lambda H^+}^2}\{\sin(\chi_{n\lambda} - \sin(\chi_{n\lambda} - A_{\lambda H^+}t) - A_{\lambda H^+}t\cos(\chi_{n\lambda} - A_{\lambda H^+}t)\} +$$

$$\frac{qE_1F(V_{He^+\alpha})}{m_{He^+}k_\perp^2} k_{II}^2 K_\perp \sum_{\lambda,n=-\infty}^{+\infty} J_\lambda(\mu) J_n(\mu) \frac{1}{A_{\lambda He^+}^2}$$

$$\{\sin(\chi_{n\lambda} - \sin(\chi_{n\lambda} - A_{\lambda He^+}t) - A_{\lambda He^+}t\cos(\chi_{n\lambda} - A_{\lambda He^+}t)\} +$$

$$\frac{qE_1F(V_{O^+})}{m_{O^+}k_\perp^2} k_{II}^2 K_\perp \sum_{\lambda,n=-\infty}^{+\infty} J_\lambda(\mu) J_n(\mu) \frac{1}{A_{\lambda O^+}^2}$$

$$\{\sin(\chi_{n\lambda} - \sin(\chi_{n\lambda} - A_{\lambda O^+}t) - A_{\lambda O^+}t\cos(\chi_{n\lambda} - A_{\lambda O^+}t)\}$$

(12)

III. DISPERSION RELATION

We consider the cold plasma dispersion relation for the ESIC wave as

$$n_{\alpha,e} = \mp \int dv F(v) \frac{eE_1K_\perp}{m_{\alpha,e}} \sum_{n\lambda} \{ J_\lambda(\mu) J_n(\mu) \times [\frac{K_\perp}{A_\lambda^2 - \Omega_\alpha^2} + \frac{k_{II}^2}{k_\perp^2 A_\lambda^2}] \sin \chi_{nl} \}$$

(13)

Where $n_{\alpha,e}$ is integrated density and

$$\mu = \frac{K_\perp V_\perp}{\Omega_{\alpha,e}}, A = K_{II}V_{II} - \omega + n\Omega_{i,e}, \chi_{n\lambda} = k.r - \omega t + (n-l)(\Omega_\alpha l - \theta)$$

Using the expression, then the dispersion relation ESIC waves in multi-component plasma is given by

$$n_e = (\frac{1}{k_\perp d_{IIe}^2}) \frac{E_1}{4\pi e} \sin(kr - \omega t)$$

And

$$n_\alpha = -\frac{k_{II}^2 \omega_{p\alpha}^2 1}{(\omega - \lambda\Omega_\alpha)k_\perp} \left\langle 1 - \frac{k_\perp^2 \rho_\alpha^2}{2} (\frac{2\kappa - 3}{\kappa}) \right\rangle \frac{E_1}{4\pi e} \sin(kr - \omega t)$$

Where $\alpha = H^+, He^+, O^+ and\ \omega_{p\alpha}^2 = \frac{4\pi N_\alpha e^2}{m_\alpha}$ is the plasma frequency for multi-ions and N_α is the multi-ions plasma density.

Debye length (d_{IIe}^2) is given by

$$d_{IIe}^2 = \frac{T_{IIe}}{m_e \omega_{pe}^2}$$

Using the Poisson's equation

$$\nabla . E = 4\pi e(n_\alpha - n_e) \quad (14)$$

The perturbed ion and electron density ni and ne the dispersion relation is obtain as

$$\omega = \Omega_\alpha + [\omega_{p\alpha}^2 \left\langle 1 - \frac{k_\perp^2 \rho_\alpha^2}{2} (\frac{2\kappa - 3}{\kappa}) \right\rangle$$

$$(\frac{1}{\frac{k_\perp}{k_{II}^2 k_\perp} + \frac{k_\perp^2}{k_{II}^2} (\frac{1}{k_\perp^2 d_{IIe}^2})})]$$

(15)

IV. WAVE ENERGY AND GROWTH RATE

The wave energy W_w per unit wavelength is the sum of the pure field energy. The total energy per unit wavelength is given as

$$W_w = \frac{\lambda B^2}{8\pi} + W_e + W_{r\alpha}$$

Where $W_e = \frac{\lambda E^2}{8\pi} + \frac{\lambda E^2}{16\pi} (\frac{1}{k_\perp d_{IIe}^2})$

$$W_{r\alpha} = \sum_\alpha (W_{r\alpha\perp} + W_{r\alpha II})$$

and

$$W_{r\perp} = \int_0^\lambda dz \int_0^\infty V_{\perp\alpha} dV_{\perp\alpha} \int_0^{2\theta} d\theta \int_{v_r - \Delta r}^{v_r + \Delta r} dV_{\Pi\alpha} \frac{m}{2} [(N + n_{1\alpha})(V_{\perp\alpha} + u_{\perp\alpha})^2 - NV_{\perp\alpha}^2]$$

(16)

$$W_{rII} = \int_0^\lambda dz \int_0^\infty V_{II\alpha} dV_{II\alpha} \int_0^{2\theta} d\theta \int_{v_r - \Delta r}^{v_r + \Delta r} dV_{\Pi\alpha} \frac{m}{2} [(N + n_{1\alpha})(V_{II\alpha} + u_{II\alpha})^2 - NV_{II\alpha}^2]$$

A. Perpendicular Resonant Energy

$$W_{r\perp\alpha} = \left(\frac{\lambda E^2}{8\pi}\right)\left(\frac{\omega_{p\alpha}^2}{\Omega_\alpha^2}\right)\left(\frac{\omega}{k_{II}V_{th\alpha}}\right)\frac{\Omega_\alpha t}{\sqrt{2\pi}}\exp$$
$$\left\{-\frac{1}{2}\left(\frac{\omega}{k_{II}V_{th\alpha}}\right)^2\left(1-\frac{\lambda\Omega_\alpha}{\omega}\right)^2\right\}\times\frac{1}{2}\left\langle 1-\frac{k^2{}_\perp\rho^2{}_\alpha}{2}\left(\frac{2\kappa-3}{\kappa}\right)\right\rangle$$
$$\left[1-\frac{R\left(\frac{\lambda\Omega_\alpha}{\omega}-1\right)}{\left(\frac{\lambda\Omega_\alpha}{\omega}\right)}\frac{T_{\perp\alpha}}{T_{II\alpha}}\right]$$

(17)

B. Parallel Resonant Energy

$$W_{rII\alpha} = \left(\frac{\lambda E^2}{8\pi}\right)\left(\frac{\omega_{p\alpha}^2}{\Omega_\alpha^2}\right)\left(\frac{\omega}{k_{II}V_{th\alpha}}\right)\frac{\Omega_\alpha t}{\sqrt{2\pi}}\exp$$
$$\left\{-\frac{1}{2}\left(\frac{\omega}{k_{II}V_{th\alpha}}\right)^2\left(1-\frac{\lambda\Omega_\alpha}{\omega}\right)^2\right\}\times\frac{1}{2}\left\langle 1-\frac{k^2{}_\perp\rho^2{}_\alpha}{2}\left(\frac{2\kappa-3}{\kappa}\right)\right\rangle$$
$$\left[1-\frac{\left(\frac{\lambda\Omega_\alpha}{\omega}-1\right)}{\left(\frac{\lambda\Omega_\alpha}{\omega}\right)}\frac{T_{\perp\alpha}}{T_{II\alpha}}\right]$$

(18)

Where

$$R = \frac{1-\frac{1}{2}\frac{k^2{}_\perp\rho^2{}_\alpha}{2}\left(\frac{2\kappa-3}{\kappa}\right)}{1-\frac{k^2{}_\perp\rho^2{}_\alpha}{2}\left(\frac{2\kappa-3}{\kappa}\right)} \text{ and } \alpha = H^+, He^+, O^+$$

C. Growth Rate

Using the law of conservation of energy the growth rate is obtained as

$$\frac{\gamma}{\omega} = \sqrt{\frac{\pi}{2}}\left(\frac{\omega}{k_{II}V_{th\alpha}}\right)\left(1-\frac{\lambda\Omega_\alpha}{\omega}\right)^2\exp\left\{-\frac{1}{2}\left(\frac{\omega}{k_{II}V_{th\alpha}}\right)^2\left(1-\frac{\lambda\Omega_\alpha}{\omega}\right)^2\right\}\times$$
$$\left[R\left(\frac{\frac{\lambda\Omega_\alpha}{\omega}-1}{\frac{\lambda\Omega_\alpha}{\omega}}\right)\frac{T_{\perp\alpha}}{T_{II\alpha}}-1\right]$$

(19)

V.RESULT AND DISCUSSIONS

A graphical depiction of the expressions is shown in Figs 1-15. The following parameters applicable to the auroral acceleration region [8-12] are used:

$B_o = 27\mu T$ at $2000km$, $\Omega_H = 412sec^{-2}$, $\Omega_{He} = 103sec^{-2}$, $\Omega_O = 26sec^{-2}$, $\frac{T_\perp}{T_\parallel} = 50$, $k_BT_\parallel = 5eV$. $k_\perp = 0.0025m^{-1}$, $\frac{T_\perp}{T_\parallel} = 5$, $k_BT_\parallel = 5eV$, $k_\parallel = 0.002\ m^{-1}$, $\omega_{pH}^2 = 1.552\times10^9 sec^{-2}$, $\omega_{pHe}^2 = .216\times10^8 sec^{-2}$, $\omega_{pO}^2 = .05\times10^8 sec^{-2}$, $k_BT_\parallel = 5eV$ And A=$\frac{T_{\perp\alpha}}{T_{\parallel\alpha}}$ for multi-ions,

here α=H^+, He^+, O^+

Fig 1 depicts that the variation of growth rate γ versus wave vector $k_\perp$ (cm^{-1}) for different values of kappa distribution k = 1, 2, 3, 4. Here it is found that growth rate is maximum at minimum value of kappa distribution corresponding to the wave vector after that it goes straight line.

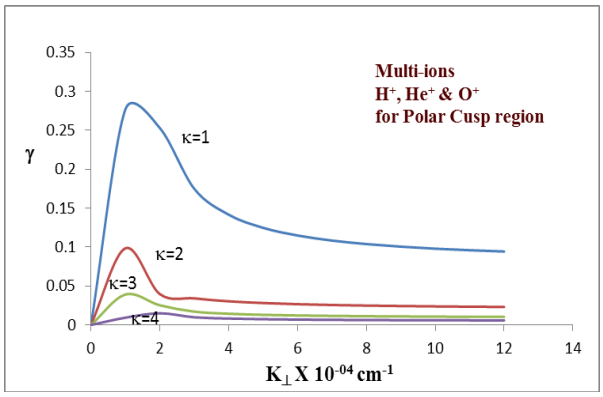

Fig 1 shows the variation of growth rate γ versus wave vector $k_\perp$ (cm^{-1}) for different values of kappa distribution k = 1, 2, 3, 4.

Fig 2, 3 show that the variation of growth rate γ versus wave vector $k_\perp$ (cm^{-1}) for different values of temperature anisotropy of hydrogen ions ($A_{H^+} = 20, 40, 60, 80$) for kappa distribution function k=1 and 2. Here we found that initially growth rate is linear then we get maximum peak of growth rate at maximum value of hydrogen temperature anisotropy. Here at the minimum value of kappa distribution, we get maximum growth rate for maximum hydrogen temperature anisotropy.

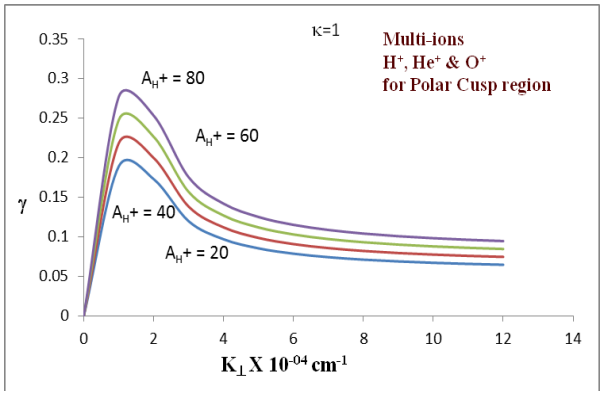

Fig 2 shows the variation of growth rate γ versus wave vector $k_\perp$ (cm^{-1}) for different values of temperature anisotropy of hydrogen ions ($A_{H^+} = 20, 40, 60, 80$) for kappa distribution function k=1.

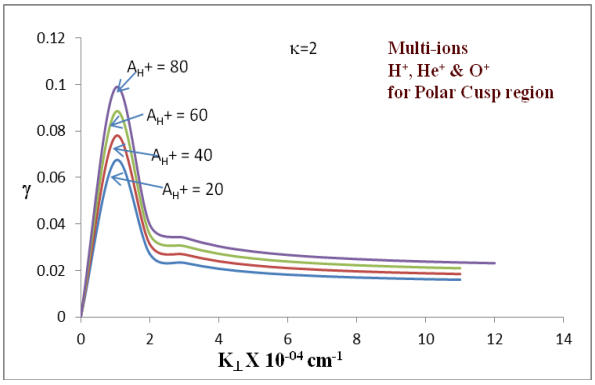

Fig 3 shows the variation of growth rate γ versus wave vector $k_\perp$ (cm^{-1}) for different values of temperature anisotropy of hydrogen ions ($A_{H^+} = 20, 40, 60, 80$) for kappa distribution function k=2.

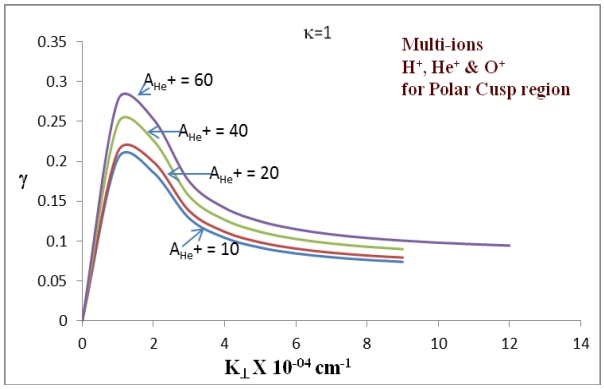

Fig 4 shows the variation of growth rate γ versus wave vector $k_\perp$ (cm^{-1}) for different values of temperature anisotropy of helium ions ($A_{He^+} = 10, 20, 40, 60$) for kappa distribution function k=1.

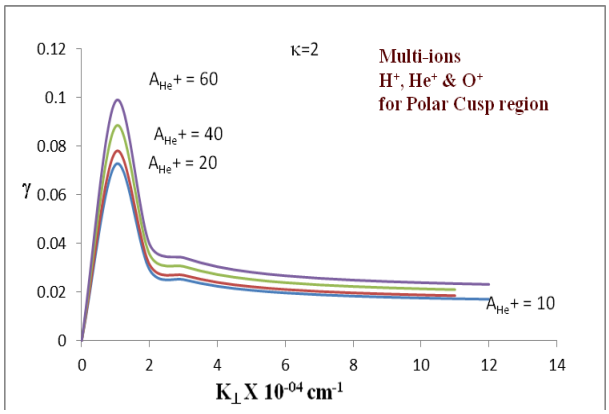

Fig 5 shows the variation of growth rate γ versus wave vector $k_\perp$ (cm^{-1}) for different values of temperature anisotropy of helium ions ($A_{He^+} = 10, 20, 40, 60$) for kappa distribution function k=2.

Fig 4, 5 show that the variation of growth rate γ versus wave vector $k_\perp$ (cm^{-1}) for different values of temperature anisotropy of helium ions ($A_{He^+} = 10, 20, 40, 60$) for kappa distribution function k=1 and 2. Here we have seen that the effect of temperature anisotropy of helium ion, growth rate is little bit minimum comparatively temperature anisotropy of hydrogen ion.

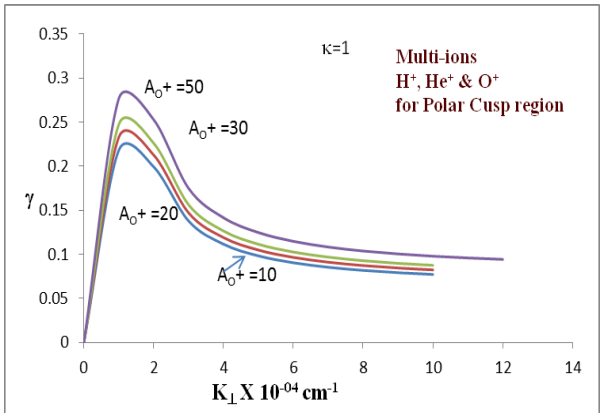

Fig 6 shows the variation of growth rate γ versus wave vector $k_\perp$ (cm^{-1}) for different values of temperature anisotropy of oxygen ions ($A_{o^+} = 10, 20, 30, 50$) for kappa distribution function k=1.

Fig 6, 7 show that the variation of growth rate γ versus wave vector $k_\perp$ (cm^{-1}) for different values of temperature anisotropy of oxygen ions ($A_{o^+} = 10, 20, 30, 50$) for kappa distribution function k=1 and 2. Here we found that initially growth rate is approximately equal for different value of temperature anisotropy of oxygen ion. Then get different peak value of growth rate at different value of oxygen temperature anisotropy. After that equal growth rate for different value of wave vector.

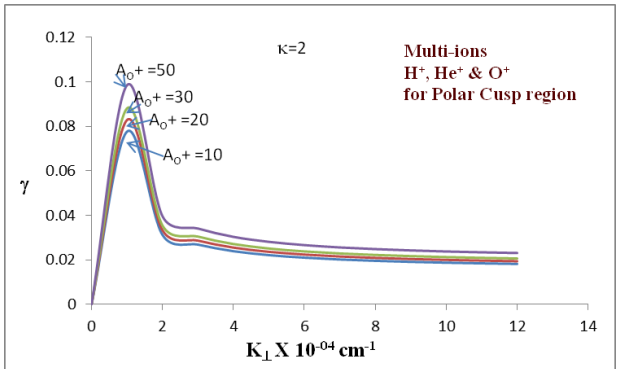

Fig 7 shows the variation of growth rate γ versus wave vector $k_\perp$ (cm^{-1}) for different values of temperature anisotropy of oxygen ions ($A_{o^+} = 10, 20, 30, 50$) for kappa distribution function k=2.

Fig 8 shows that the Variation of perpendicular resonant energy $W_{r\perp}$(erg cm) versus perpendicular wave vector $K_\perp$ (cm^{-1}) for different values of kappa distribution function (k=1, 2, 3 and 4). Here we found for k=1 and 2 we get no perpendicular resonant energy. As we increase the value of kappa(k= 3 and 4),it get negative perpendicular resonant energy. It implies that at maximum value of kappa we get minimum resonant energy.

Fig 9-11 show that the variation of perpendicular resonant energy (erg cm) versus wave vector (cm^{-1}) for different values of plasma densities of hydrogen, helium and oxygen ions ($n_{H^+}\ or\ n_{He^+}\ or\ n_{o^+} = 100, 200, 300, 500$) cm^{-3} for kappa distribution function k=1. For minimum value of hydrogen plasma density we get no resonant energy. As we increase the value of hydrogen plasma density, we get increasing resonant energy. But for minimum helium plasma densitywe get minimum resonant energy. As we increase the value of plasma density of helium, we get maximum perpendicular resonant energy. And for oxygen plasma density, we get increasing resonant energy. We found that as we increase the value of plasma density of oxygen, we get maximum resonant energy. But in fig 9-11 we have seen that for hydrogen plasma density we get maximum resonant energy.

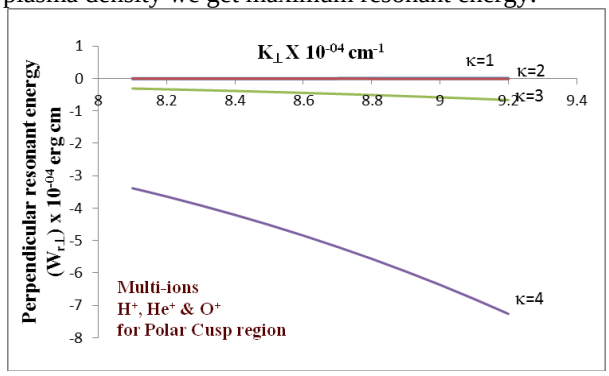

Fig 8 shows the Variation of perpendicular resonant energy $W_{r\perp}$(erg cm) versus perpendicular wave vector $K_\perp$ (cm^{-1}) for different values of kappa distribution function (k=1, 2, 3 and 4).

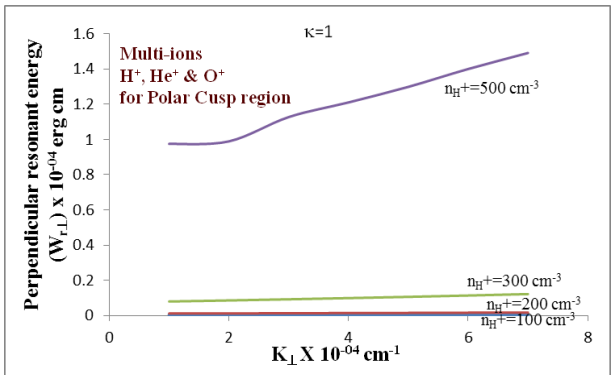

Fig 9 shows the variation of perpendicular resonant energy (erg cm) versus wave vector (cm^{-1}) for different values of plasma densities of hydrogen ions ($n_{H^+} = 100, 200, 300, 500$) cm^{-3} for kappa distribution function k=1.

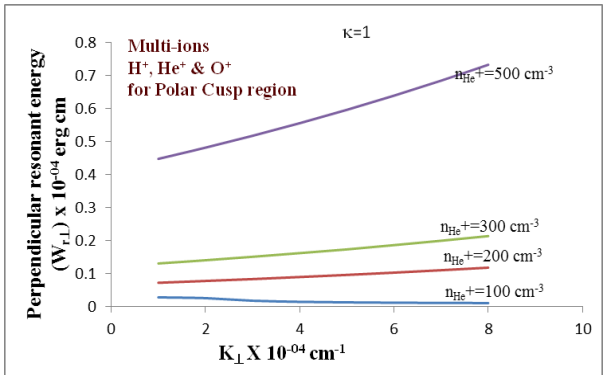

Fig 10 shows the variation of perpendicular resonant energy (erg cm) versus wave vector (cm^{-1}) for different values of plasma densities of helium ions ($n_{He^+} = 100, 200, 300, 500$) cm^{-3} for kappa distribution function k=1.

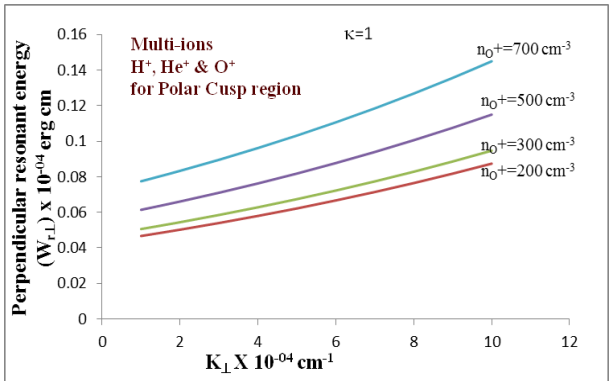

Fig 11 shows the variation of perpendicular resonant energy (erg cm) versus wave vector (cm^{-1}) for different values of plasma densities of oxygen ions ($n_{o^+} = 200, 300, 500, 700$) cm^{-3} for kappa distribution function k=1.

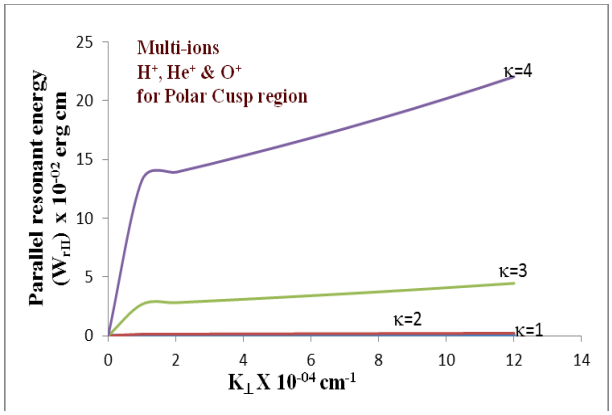

Fig 12 shows the Variation of parallel resonant energy $W_{r\parallel}$(erg cm) versus perpendicular wave vector $K_\perp$ (cm^{-1}) for different values of kappa distribution function (k=1, 2, 3 and 4).

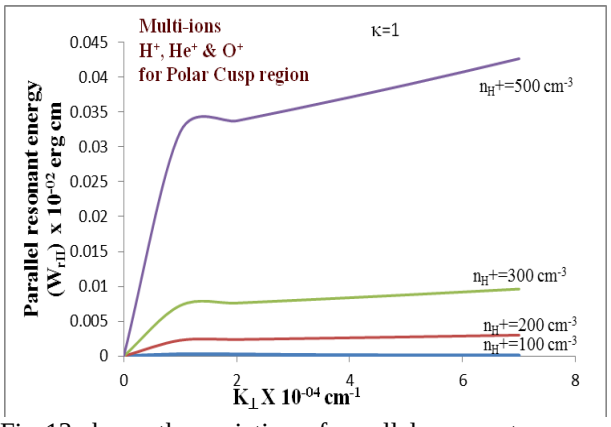

Fig 13 shows the variation of parallel resonant energy (erg cm) versus wave vector (cm^{-1}) for different values of plasma densities of hydrogen ions ($n_{H^+} = 100, 200, 300, 500$) cm^{-3} for kappa distribution function k=1.

Fig 12 shows that the Variation of parallel resonant energy $W_{r\parallel}$(erg cm) versus perpendicular wave vector $K_\perp$ (cm^{-1}) for different values of kappa distribution function (k=1, 2, 3 and 4). Initially it is found that for k=1 and 2, there is no parallel resonant energy. As we increase the value of kappa we get increasing parallel resonant energy for different value of wave vector.

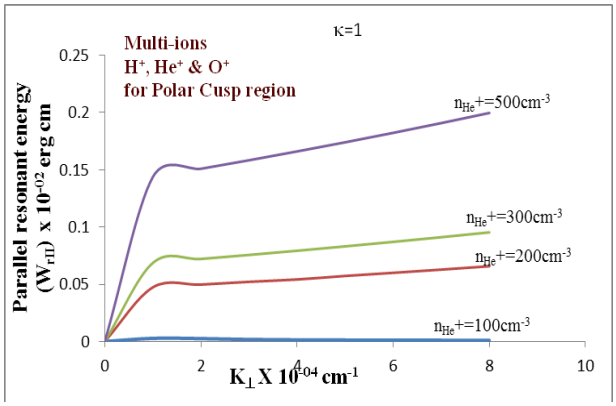

Fig 14 shows the variation of parallel resonant energy (erg cm) versus wave vector (cm^{-1}) for different values of plasma densities of helium ions ($n_{He^+} = 100, 200, 300, 500$) cm^{-3} for kappa distribution function k=1.

Fig 13-15 show that the variation of parallel resonant energy (erg cm) versus wave vector (cm^{-1}) for different values of plasma densities of hydrogen, helium and oxygen ions (n_{H^+} or n_{He^+} or $n_{o^+} = 100, 200, 300, 500$) cm^{-3} for kappa distribution function k=1. Here we have equivalent nature of parallel resonant energy for all plasma densities. It means initially resonant energy is zero for hydrogen and helium plasma densities. After that as we increase the plasma densities we get initially linear then slightly increasing resonant energy with respect to wave vector. But for oxygen plasma densities, resonant energy is initially linear then increasing with respect to wave vector. Here we observed for helium plasma densities we get maximum parallel resonant energy with respect to the wave vector. This is in accordance with the preservation of energy in mirror-like campaigns.

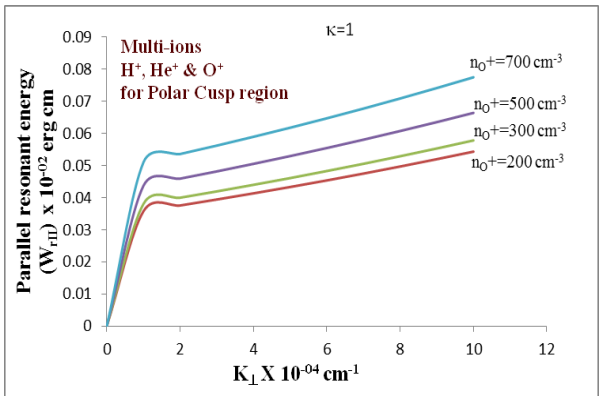

Fig 15 shows the variation of parallel resonant energy (erg cm) versus wave vector (cm^{-1}) for different values of plasma densities of oxygen ions ($n_{o^+} = 200, 300, 500, 700$) cm^{-3} for kappa distribution function k=1.

Hence, a moment agoperceived ESIC waves in multi-ions plasma by several satellites in the cusp region along with kappa distribution of particles due to mirror-like geometry of cusp region may act as a probable source to give rise to the detected ESIC in the cusp region through the wave-particle resonant interaction appliance.

VI. CONCLUSION

The outcomes of present work are following:

- The effect of kappa distribution function is to enhance the growth rate with respect to wave vector.
- At maximum temperature anisotropy of hydrogen, helium and oxygen ions we get maximum growth rate but for the value of kappa k = 1, the nature of growth rate almost same for different value of plasma densities and for k = 2, the nature of growth rate is same for all values of plasma densities of different ions.
- At increasing value of kappa, we get minimum perpendicular resonant energy.

- The effect of different plasma densities of ions is to enhance the perpendicular resonant energy with respect to wave vector.
- The increasing value of kappa we get maximum parallel resonant energy.
- The effect of different plasma densities of ions is to enhance the parallel resonant energy with respect to wave vector.

The status of this effort may be prominence in the electrostatic emission in the polar cusp region. The outcome of the study is also relevant to the plasma campaigns that consume kappa distribution.

REFERENCES

[1] Bouhram M, Dubouloz N, Malingre M, Jasperse J R, Pottelette R, Senior C, Delcourt D, Carlson C W, Roth I Berthomier M &Sauvaud J A, J Geophys Res, 107 (2002) 10.1029/2001 JA000091.

[2] Andre M, Keskinen H, Gustafsson G &Lundin R, Geophys Res Lett, 14 (1987) 463.

[3] Sundkvist D, Vaivads A, Andre M, Wahlund J-E, Hobara Y, Joko S, Krasnoselskikh V V, Bogdanova Y V, Buchert S C, Cornilleau-Wehrlin N, Fazakerley A, Hall J-O, Reme H &Stenberg G, AnnalesGeophysicae, 23 (2005) 983.

[4] Tiwari M S &Varma P, Planet Space Sci, 41 (1993) 199.

[5] Mishra R & Tiwari M S, Ind J Pure &ApplPhys, 42 (2004) 104; Ind J Pur&ApplPhys, 43 (2005) 377; Planet Space Sci, 54 (2006) 188.

[6] Mishra R & Tiwari M S, Earth, Moon & Planets, 100 (2007) 195.

[7] Terashima Y, ProgTheorPhys, 37 (1967) 661.

[8] Bouhram M, Dubouloz N, Malingre M, Jasperse J R, Pottelette R, Senior C, Delcourt D, Carlson C W, Roth I,

[9] Berthomier M &Sauvaud J A, J Geophys Res, 107 (2002) 10.1029/2001 JA000091.

[10] Mishra, R and M S Tiwari, (2006), Effect of parallel electric field on electrostatic ion cyclotron instability in anisotropic plasma in the presence of ion beam and general distribution function, Planet. Space Sci**., 54**, 188.

[11] Tiwari, M. S. and Rostoker, G.: Field aligned currents and auroral acceleration by non-linear MHD waves, Planet. Space Sci., 32, 1497–1503, 1984.

[12] Mozer F S, Ergun R, Temrin M, Cattell C, Donsbeeck J &Wygant J, Phys Rev Lett, 79 (1997) 1281.

[13] Duan, S. P., Li, Z. Y., and Liu, Z. X.: Kinetic Alfv´en wave driven by the density inhomogeneity in the presence of loss-cone distribution function-Particle aspect analysis, Planet. Space Sci., 53, 1167–1173, 2005.